

1 **SUPPLEMENTAL INFORMATION**

2 **Methods and Materials**

3 *Estimating environmental parameters for modern brachiopod samples*

4 We used bathymetric maps to estimate depths for specimens lacking those data, assigning
5 depths from most likely brachiopod habitat for each locality (i.e. hard substrates in atlases). We
6 derived habitat temperature and salinity from the World Ocean Atlas 2013 (Locarnini et al.,
7 2013; Zweng et al., 2013) and carbonate chemistry parameters from the GLODAP v2 database
8 (National Center for Atmospheric Research Staff (Eds), 2014). We used CO2Calc to calculate
9 habitat pH from estimated carbonate chemistry data (Robbins et al., 2010). Due to some
10 specimens' uncertain sampling depths, use of atlases to infer environmental conditions, and
11 potential seasonal variability, we assign temperature estimates large uncertainties ($\pm 2^{\circ}\text{C}$). We
12 further recognize the considerable uncertainty inherent in using gridded datasets to infer the
13 parameters that are highly heterogeneous in natural environments, and we recommend future
14 work on modern brachiopods with well-constrained growth conditions, ideally also including
15 direct constraints on growth rates.

16

17 *Screening samples for alteration and contamination*

18 Reliable geochemical analysis of carbonate samples depends on avoiding contamination
19 (which typically can come from trace silicate or Fe-Mn oxide phases) and selecting well
20 preserved material that has not had its composition altered during diagenesis. Although
21 brachiopods are generally well-suited as geochemical archives (e.g., Veizer et al., 1999), careful
22 screening remains important for yielding reliable isotopic reconstructions (e.g., Buening, 2001).

23 We screened for silicate and oxide contamination based on element-to-calcium ratios,
24 particularly focusing on Al to trace silicate leaching following established approaches. Published
25 data from experiments using carbonate-rich samples suggest that $\delta^7\text{Li}$ values for leachates with
26 $\text{Al}/\text{Ca} > 800 \mu\text{mol}/\text{mol}$ might reflect silicate leaching (Pogge von Strandmann et al., 2013). More
27 recent work on the effect of leaching procedures on $\delta^7\text{Li}$ values for samples with varying
28 carbonate-to-silicate ratios suggests that Al/Ca limits vary based on phases present in sample
29 matrices (Bastian et al., 2018). For this work, we expect that brachiopod shells should be
30 carbonate-dominated and so adopt a conservative Al/Ca limit of $300 \mu\text{mol}/\text{mol}$ to identify
31 modern and fossilized brachiopod leachates with possible silicate contamination. We therefore
32 exclude samples with Al/Ca ratios that exceed this cutoff (Pogge von Strandmann, 2008). This
33 criterion led us to exclude one modern sample (with $\text{Al}/\text{Ca} = 1146.2 \mu\text{mol}/\text{mol}$) and four fossil
34 samples (Fig. S2). Modern specimen Mn/Ca and Fe/Ca values were also monitored to determine
35 the influence of possible Fe-Mn oxide leaching; with the exception of the craniid specimen
36 (M34), we found no evidence for elevated values of these ratios in our data (Table A1).

37 We combined multiple approaches to screen fossil specimens for diagenetic alteration prior
38 to analysis (Fig. S2), informed by past work on other isotope systems in brachiopods. The
39 diagenetic alteration of brachiopod geochemical signatures is recognized as being complex, and
40 no one single method has proven successful in distinguishing alteration in all cases (Buening,
41 2001) — motivating our multi-pronged approach. We began by assessing microstructure
42 preservation with scanning electron microscopy (SEM) and evaluating trace element
43 incorporation based on cathodoluminescence (CL) microscopy (Figs. S3 and S4 show
44 representative CL and SEM images, respectively).

45 We complemented the microscopy observations with geochemical evaluation. We used
46 measured radiogenic Sr isotope ratios, recognizing that resetting of Sr composition in carbonates
47 is likely to imply resetting of the Li system as well (Dellinger et al., 2020). We excluded fossil
48 samples with more than ~10ppm difference between the measured $^{87}\text{Sr}/^{86}\text{Sr}$ value and that
49 expected based on the seawater curve (McArthur et al., 2012), based on the age range known for
50 each specimen from stratigraphy.

51 Diagenetic alteration was also evaluated based on Mn/Sr values, using $\text{Mn/Sr} > 1\text{mol/mol}$ as
52 a threshold indicative of alteration (Veizer, 1983). While Mn/Sr ratios (as well as Mn/Ca and
53 Sr/Ca ratios) have been used extensively to investigate carbonate diagenesis, it has been
54 suggested that these ratios be used cautiously to screen macro-fossils such as brachiopods
55 (Ullmann and Korte, 2015). In particular, diagenetic setting and fossil type should be considered
56 when interpreting these ratios. Additionally, studies of modern brachiopod shells reveal
57 variability in Mn/Ca and Sr/Ca ratios between different brachiopod taxa as well as within
58 individual shells, which has been attributed to environmental conditions, shell growth rates,
59 and/or varying growth mechanisms between shell layers (Ullmann et al. 2017; Rollion-Bard et
60 al. 2019), potentially complicating the use of these element ratios for diagenetic screening. More
61 work is needed to understand the relationship between environmental, physiological, and
62 diagenetic factors that might influence Mn/Sr, Li/Ca, and Li isotope compositions of
63 brachiopods.

64 An important consideration in using geochemical indices for diagenetic screening is that
65 trace elements like Mn or Sr in a brachiopod shell may not necessarily reflect alteration of Li and
66 its isotopes, especially if these elements may have different distributions within shells. Variable
67 Li/Ca ratios have been observed in modern brachiopod primary layers and attributed to

68 complexity of the calcification mechanism, whereas secondary layers are more internally
69 consistent within shells (Rollion-Bard et al., 2019). These observations lend some confidence to
70 the use of secondary layers for Li analysis, although data on isotope distributions within
71 brachiopod shells layers remains lacking — reflecting a worthwhile target for future work. If Li
72 isotope compositions are heterogeneous within secondary layers, then preferential dissolution
73 and loss of Li from isotopically distinct carbonate could influence measured bulk $\delta^7\text{Li}$ in ways
74 that may not be picked up by trace element ratios. However, we would expect to see signs of
75 such dissolution in SEM images, emphasizing the importance of combining multiple approaches
76 to evaluating potential alteration.

77 Altogether, we identified alteration in 15 of the 41 leachates we analyzed (Fig. S2, and
78 details in Table A2). Note that only two data points (UF1 and UF1 dup) were excluded based on
79 the basis of Mn/Sr ratios, and these data are from duplicate measurements of the same specimen
80 that showed signs of a high degree of alteration under SEM. Thus, while there is certainly room
81 to improve understanding of the Li isotope preservation in brachiopods, we suggest that use of
82 multiple screening approaches including detailed microscopy, Sr isotope stratigraphy, and trace
83 element ratios provides a general framework that may be refined as more is learned in the future.

84

85 **Brachiopod Biomineralization and Potential Effects on $\delta^7\text{Li}$**

86 Given the lack of any clear relationship between $\delta^7\text{Li}$ compositions of brachiopods and
87 their environmental conditions (Fig. 2), at least within the data from this study, another control
88 on $\delta^7\text{Li}$ fractionation must be invoked. Effects associated with biomineralization are one
89 possibility. In part because fossil specimens dominate research thus far on the phylum,

90 brachiopod biomineralization is incompletely understood. Proteomic studies suggest that,
91 relative to other marine calcifiers, brachiopods precipitate their shells using a novel molecular
92 mechanism. In the process, they might utilize an enzyme similar to that found in corals (α -
93 carbonic anhydrase) to increase calcite precipitation rate (Jackson et al., 2015; Immel et al.,
94 2015; Isowa et al., 2015). The secondary shell layer, most commonly used for reconstructions of
95 paleoenvironmental conditions, is composed of calcite fibers that behave optically like single
96 calcite crystals (Pérez-Huerta et al., 2018). Through many studies of brachiopod shell structure,
97 Williams proposed that the different layers of the shell are produced by a single cell via a
98 conveyor belt system (Williams, 1953, 1966, 1968a, 1968b; Williams and Rowell, 1965). In
99 contrast, a recent study proposed that more than one cell participates in the precipitation of a
100 single calcite fiber/crystal, suggesting that calcite fibers are formed via ion transport of calcium
101 (along with trace/minor elements) and carbonate rather than forming elsewhere in the epithelium
102 and being transported and secreted by cell vacuoles (Simonet Roda et al., 2019). Additionally,
103 while Simonet Roda et al. (2019) did not find evidence of a metastable, amorphous calcium
104 carbonate (ACC) precursor to brachiopod calcite, ACC has been observed in one study of a
105 rhynchonelliform brachiopod (Griesshaber et al., 2009), while other researchers found that
106 brachiopod shell fibers are composed of calcite nanospheres or granules. Within the order
107 Terebratulida, triangular particles are present, which have not been observed in any other known
108 calcifying organisms (Cusack et al., 2008; Pérez-Huerta et al., 2013).

109 Environmental conditions and/or trace element ratios may offer some insight into how
110 biomineralization influences Li incorporation into brachiopod shells (Fig. S9). While there are no
111 significant correlations between Li/Ca ratios and calculated habitat [DIC] or pH, Li/Ca ratios for
112 all rhynchonelliform specimens in this study are positively correlated with Sr/Ca ratios ($r^2 = 0.4$).

113 However, Li/Ca ratios do not significantly correlate with Mg/Ca ratios, which is surprising given
114 the similar ionic radii of Li and Mg. The relationship between Li/Ca and Sr/Ca may be due to the
115 affinity for both Li^+ and Sr^{2+} to incorporate into calcite during rapid crystal growth. Theoretical
116 studies suggest relationships between Li/Ca and Sr/Ca may emerge because imperfections at
117 crystal surfaces are “entrapped” when calcite grows quickly, and Li and Sr share a high affinity
118 for these traps; this is referred to as the growth entrapment model or GEM (Watson and Liang,
119 1995; Watson, 1996, 2004; DePaolo, 2011).

120 In contrast to Li/Ca, $\delta^7\text{Li}$ compositions are weakly negatively correlated with both their
121 Sr/Ca ($r^2 = 0.18$) and Mg/Ca ($r^2 = 0.17$) ratios. While these are weak correlations, they suggest
122 mechanisms controlling Sr and Mg incorporation into brachiopod shells might also influence Li
123 isotope fractionation during shell formation. Although evidence for an ACC precursor in
124 brachiopods is equivocal (see above), it could provide one explanation for the observed
125 elemental behavior. Mg^{2+} and Sr^{2+} incorporation into calcite via ACC crystallization results in
126 distortions of the crystal lattice. These distortions in turn affect the surrounding bonding
127 environments. At high Mg^{2+} concentrations, Sr^{2+} inhabits a 9-fold coordination versus
128 substituting for Ca^{2+} in smaller, more stable 6-fold coordination sites (Littlewood et al., 2017). If
129 Sr^{2+} and Mg^{2+} were to distort the calcite crystal lattice in the presence of Li^+ , while Li^+ might
130 normally inhabit a 6-fold coordination, some Li^+ ions might be trapped in 9-fold coordination.
131 Given that Li is strongly bound in a tetrahedra of -OH groups in water (Olsher et al., 1991),
132 when it coprecipitates with calcite, the bonding environment should greatly impact how the
133 isotopes of Li fractionate. Given that the tetrahedral bonding environment is strongest versus
134 octahedral or orthorhombic environments in calcite, the lighter isotope of Li has a greater affinity
135 for the solid phase. This is supported by studies of Li isotopes in inorganically precipitated

136 calcite and aragonite – the $\delta^7\text{Li}$ of the solid phases is always lower than the fluid from which
137 they precipitated, with aragonite having a lower isotopic composition than calcite likely due to Li
138 inhabiting weaker bonding sites in aragonite than in calcite or water (Marriott et al., 2004b,
139 2004a; Gabitov et al., 2011). Thus, the bonding of Li in 9-fold coordination sites, driven by the
140 presence of distortions from Sr and Mg, could potentially explain why some brachiopod shells
141 have lighter $\delta^7\text{Li}$. Alternatively, faster diffusion of ^6Li versus ^7Li into calcification sites might
142 explain the tendency towards lighter compositions as Li is trapped if there is rapid crystal
143 growth. Verifying these proposed mechanisms, as well as evaluating how dependencies of shell
144 $\delta^7\text{Li}$ on growth rates or conditions, would clearly require further work.

145 **REFERENCES FOR SUPPLEMENTAL TEXT AND FIGURES S1-S9**

- 146 Bastian, L., Vigier, N., Reynaud, S., Kerros, M.-E., Revel, M., and Bayon, G., 2018, Lithium
147 Isotope Composition of Marine Biogenic Carbonates and Related Reference Materials:
148 Geostandards and Geoanalytical Research, v. 42, p. 403–415, doi:10.1111/ggr.12218.
- 149 Buening, 2001, Brachiopod Shells: Recorders of the Present and Keys to the Past. In:
150 Brachiopods Ancient and Modern: A Tribute to G. Arthur Cooper, Paleontological Society
151 Papers v.7, pp. 117-144.
- 152 Cusack, M., Dauphin, Y., Chung, P., Pérez-Huerta, A., and Cuif, J.-P., 2008, Multiscale structure
153 of calcite fibres of the shell of the brachiopod *Terebratulina retusa*: Journal of Structural
154 Biology, v. 164, p. 96–100, doi:10.1016/j.jsb.2008.06.010.
- 155 DePaolo, D.J., 2011, Surface kinetic model for isotopic and trace element fractionation during
156 precipitation of calcite from aqueous solutions: Geochimica et Cosmochimica Acta, v.
157 75, p. 1039–1056.
- 158 Gabitov, R.I., Schmitt, A.K., Rosner, M., McKeegan, K.D., Gaetani, G.A., Cohen, A.L., Watson,
159 E.B., and Harrison, T.M., 2011, In situ $\delta^7\text{Li}$, Li/Ca, and Mg/Ca analyses of synthetic
160 aragonites: Geochemistry, Geophysics, Geosystems, v. 12.
- 161 Griesshaber, E., Kelm, K., Sehrbrock, A., Mader, W., Mutterlose, J., Brand, U., and Schmahl,
162 W.W., 2009, Amorphous calcium carbonate in the shell material of the brachiopod
163 *Megerlia truncata*: European Journal of Mineralogy, v. 21, p. 715–723, doi:10.1127/0935-
164 1221/2009/0021-1950.
- 165 Hall, J.M., Chan, L.-H., McDonough, W.F., and Turekian, K.K., 2005, Determination of the
166 lithium isotopic composition of planktic foraminifera and its application as a paleo-seawater
167 proxy: Marine Geology, v. 217, p. 255–265.
- 168 Immel, F., Gaspard, D., Marie, A., Guichard, N., Cusack, M., and Marin, F., 2015, Shell
169 proteome of rhynchonelliform brachiopods: Journal of Structural Biology, v. 190, p. 360–
170 366, doi:10.1016/j.jsb.2015.04.001.
- 171 Isowa, Y., Sarashina, I., Oshima, K., Kito, K., Hattori, M., and Endo, K., 2015, Proteome
172 analysis of shell matrix proteins in the brachiopod *Laqueus rubellus*: Proteome Science,
173 v. 13, doi:10.1186/s12953-015-0077-2.
- 174 Jackson, D.J., Mann, K., Häussermann, V., Schilhabel, M.B., Lüter, C., Griesshaber, E.,
175 Schmahl, W., and Wörheide, G., 2015, The *Magellania venosa* biomineralizing proteome: a
176 window into brachiopod shell evolution: Genome Biology and Evolution, v. 7, p. 1349–
177 1362.
- 178 Littlewood, J.L., Shaw, S., Peacock, C.L., Bots, P., Trivedi, D., and Burke, I.T., 2017,
179 Mechanism of Enhanced Strontium Uptake into Calcite via an Amorphous Calcium
180 Carbonate Crystallization Pathway: Crystal Growth & Design, v. 17, p. 1214–1223,
181 doi:10.1021/acs.cgd.6b01599.

- 182 Locarnini, R.A. et al., 2013, World Ocean Atlas 2013, Volume 1: Temperature: NOAA National
183 Environmental Satellite, Data, and Information Service.
- 184 Marriott, C.S., Henderson, G.M., Belshaw, N.S., and Tudhope, A.W., 2004a, Temperature
185 dependence of $\delta^{7}\text{Li}$, $\delta^{44}\text{Ca}$ and Li/Ca during growth of calcium carbonate: Earth and
186 Planetary Science Letters, v. 222, p. 615–624.
- 187 Marriott, C.S., Henderson, G.M., Crompton, R., Staubwasser, M., and Shaw, S., 2004b, Effect of
188 mineralogy, salinity, and temperature on Li/Ca and Li isotope composition of calcium
189 carbonate: Chemical Geology, v. 212, p. 5–15.
- 190 National Center for Atmospheric Research Staff (Eds), 2014, GLODAP: GLObal Ocean Data
191 Analysis Project for Carbon | NCAR - Climate Data Guide:,
192 [https://climatedataguide.ucar.edu/climate-data/glodap-global-ocean-data-analysis-project-](https://climatedataguide.ucar.edu/climate-data/glodap-global-ocean-data-analysis-project-carbon)
193 [carbon](https://climatedataguide.ucar.edu/climate-data/glodap-global-ocean-data-analysis-project-carbon) (accessed December 2018)
- 194 Olsher, Uriel., Izatt, R.M., Bradshaw, J.S., and Dalley, N.Kent., 1991, Coordination chemistry of
195 lithium ion: a crystal and molecular structure review: Chemical Reviews, v. 91, p. 137–
196 164, doi:10.1021/cr00002a003.
- 197 Pérez-Huerta, A., Coronado, I., and Hegna, T.A., 2018, Understanding biomineralization in the
198 fossil record: Earth-Science Reviews, v. 179, p. 95–122,
199 doi:10.1016/j.earscirev.2018.02.015.
- 200 Pérez-Huerta, A., Dauphin, Y., and Cusack, M., 2013, Biogenic calcite granules—Are
201 brachiopods different? Micron, v. 44, p. 395–403, doi:10.1016/j.micron.2012.09.005.
- 202 Pogge von Strandmann, P.A., 2008, Precise magnesium isotope measurements in core top
203 planktic and benthic foraminifera: Geochemistry, Geophysics, Geosystems, v. 9.
- 204 Robbins, L.L., Hansen, M.E., Kleypas, J.A., and Meylan, S.C., 2010, CO2calc: A user-friendly
205 seawater carbon calculator for Windows, Mac OS X, and iOS (iPhone): US Geological
206 Survey.
- 207 Rollion-Bard, C., Garcia, S.M., Burckel, P., Angiolini, L., Jurikova, H., Tomašových, A., and
208 Henkel, D., 2019, Assessing the biomineralization processes in the shell layers of modern
209 brachiopods from oxygen isotopic composition and elemental ratios: Implications for their
210 use as paleoenvironmental proxies: Chemical Geology, v. 524, p. 49–66.
- 211 Simonet Roda, M. et al., 2019, Calcite fibre formation in modern brachiopod shells: Scientific
212 Reports, v. 9, doi:10.1038/s41598-018-36959-z.
- 213 Ullmann, C.V., Frei, R., Korte, C., and Lüter, C., 2017, Element/Ca, C and O isotope ratios in
214 modern brachiopods: Species-specific signals of biomineralization: Chemical Geology, v.
215 460, p. 15–24, doi:10.1016/j.chemgeo.2017.03.034.
- 216 Ullmann, C.V., and Korte, C., 2015, Diagenetic alteration in low-Mg calcite from macrofossils: a
217 review: Geological Quarterly, v. 59, p. 3–20, doi: 10.7306/gq. 1217.

- 218 Watson, E.B., 2004, A conceptual model for near-surface kinetic controls on the trace-element
219 and stable isotope composition of abiogenic calcite crystals 1 Associate editor: R.H.
220 Byrne: *Geochimica et Cosmochimica Acta*, v. 68, p. 1473–1488, doi:10.1016/j.gca.2003.10.003.
- 221 Watson, E.B., 1996, Surface enrichment and trace-element uptake during crystal growth:
222 *Geochimica et Cosmochimica Acta*, v. 60, p. 5013–5020.
- 223 Watson, E.B., and Liang, Y., 1995, A simple model for sector zoning in slowly grown crystals:
224 Implications for growth rate and lattice diffusion, with emphasis on accessory minerals in
225 crustal rocks: *American Mineralogist*, v. 80, p. 1179–1187.
- 226 Williams, A., 1968a, A history of skeletal secretion among articulate brachiopods: *Lethaia*, v. 1,
227 p. 268–287.
- 228 Williams, A., 1968b, Evolution of the shell structure of articulate brachiopods: *Special Papers in*
229 *Palaeontology*, v. 2, p. 1–55.
- 230 Williams, A., 1966, Growth and structure of the shell of living articulate brachiopods: *Nature*, v.
231 211, p. 1146.
- 232 Williams, A., 1953, North American and European Stropheodontids: their morphology and
233 systematics: *Geological Society of America*, v. 56.
- 234 Williams, A., and Rowell, A., 1965, *Treatise on invertebrate paleontology. H. Brachiopoda: Part*
235 *H*, v. 1.
- 236 Zweng, M.M. et al., 2013, *World Ocean Atlas 2013, Volume 2: Salinity*: NOAA National
237 *Environmental Satellite, Data, and Information Service*.

238 **Supplemental Figure Captions**

239 **Figure S1:** Bulk brachiopod $\delta^7\text{Li}$ compositions from this study and Dellinger et al. (2018) and
240 primary layer brachiopod $\delta^7\text{Li}$ compositions by genus from this study (Dellinger et al., 2018).
241 Symbols are the same as in Fig. 1, with the addition of new symbols for primary layer
242 compositions measured in this study.

243

244 **Figure S2:** Circled samples are removed from the reconstruction of past seawater $\delta^7\text{Li}$
245 composition based on the specified screening criteria: A) $\text{Mn/Sr} > 1000$ mmol/mol, B)
246 differences between sample $^{87}\text{Sr}/^{86}\text{Sr}$ ratios over their stratigraphic age ranges relative to the
247 marine $^{87}\text{Sr}/^{86}\text{Sr}$ LOWESS fit curve in ppm, as shown in Figure A1 (McArthur et al., 2012); C)
248 Al/Ca ratios > 300 $\mu\text{mol/mol}$; D) samples showing signs of poor preservation under SEM. Most
249 specimens with poor preservation based on SEM images also show signs of diagenetic alteration
250 based on criteria A-C, but one specimen, NZ4, was only excluded based on SEM images. See
251 Figure S5 for the image of NZ4.

252

253 **Figure S3:** Cathodoluminescent images of fossilized brachiopods with varying degrees of
254 alteration, revealed by greater luminescence. All images were made with a 2 second exposure
255 time. More intense luminescence corresponds to more Mn and Fe in the calcite (Machel, 2000)

256

257 **Figure S4:** Scanning Electron Microscope images of fossilized brachiopods with varying
258 degrees of preservation. Images in the first row are characteristic of well-preserved specimens,
259 and images in the second row are representative of poorly preserved specimens. For specimens

260 from the Rhynchonellata class, suitable specimens have preservation of microstructures like
261 fibrous secondary shell layer and prismatic tertiary layers (Garbelli et al., 2012, 2014).
262 Separation of fibers or laminae potentially allows for fluids to flow through the shell, increasing
263 the likelihood of diagenetic alteration, while amalgamation of secondary and/or tertiary layer
264 fibers is indicative of alteration.

265

266 **Figure S5:** Fossil brachiopod Li isotope compositions over the past 70 Ma differentiated by
267 taxonomic group. There is no systematic variability in Li isotope values when comparing
268 different taxa with overlapping ages.

269

270 **Figure S6:** Relationship between modern brachiopod Li/Ca ratios and habitat temperature. Open
271 symbols represent specimens without depth data. Lines show exponential fits through data as
272 noted in the legend. In addition to the Li/Ca data from Dellinger et al. (2018) and this study, the
273 plot includes data from Delaney et al. (1989) who reported Li/Ca ratios on selected brachiopod
274 samples but not Li isotope compositions; therefore the equivalent samples do not appear on Fig.
275 2 of the main text. For the data from Delaney et al. (1989) and this study, specimens in the genus
276 *Tichosina* are not included in the Li/Ca – Temperature calibrations. Note that, as reported in
277 prior studies (both for foraminifera and brachiopods), there is an apparent temperature effect on
278 Li/Ca ratios but not on Li isotope ratios.

279

280 **Figure S7:** $^{87}\text{Sr}/^{86}\text{Sr}$ ratios for fossilized brachiopods and the marine $^{87}\text{Sr}/^{86}\text{Sr}$ LOWESS Fit
281 curve (McArthur et al., 2012). The lower figure includes all samples, while the upper figure

282 shows a subset of samples with $^{87}\text{Sr}/^{86}\text{Sr}$ between 0.7075 and 0.7095. Samples with $^{87}\text{Sr}/^{86}\text{Sr}$
283 ratios and stratigraphic ages that do not align with the marine $^{87}\text{Sr}/^{86}\text{Sr}$ record within analytical
284 uncertainty are labeled and are excluded from the reconstruction of Cenozoic brachiopod $\delta^7\text{Li}$ in
285 Figure 3.

286

287 **Figure S8:** A) Fossil brachiopod $\delta^7\text{Li}$ values over the past ~70 Ma. Blue rectangles are data from
288 this study and gray circles are published foraminifer data (Misra and Froelich, 2012). Rectangle
289 widths are ages from stratigraphy and $^{87}\text{Sr}/^{86}\text{Sr}$ values; heights reflect $\delta^7\text{Li}$ 1σ analytical
290 uncertainty. B) Cenozoic seawater $\delta^7\text{Li}$ values from adding fractionation factors of 4‰ (this
291 study) and 1‰ (Hall et al., 2005) to brachiopod and foraminifer $\delta^7\text{Li}$ values, respectively.

292

293 **Figure S9:** Relationships between Li/Ca ratios and A) calculated habitat pH, B) calculated
294 habitat [DIC], C) Sr/Ca ratios, and D) Mg/Ca ratios for rhynchonelliform brachiopods. Data from
295 Dellinger et al. (2018) are included when available (Dellinger et al., 2018). Symbols are the same
296 as those previously described. There are no correlations between Li/Ca and pH, [DIC], or
297 Mg/Ca, but there is a weak correlation between shell bulk shell Li/Ca and Sr/Ca ratios.

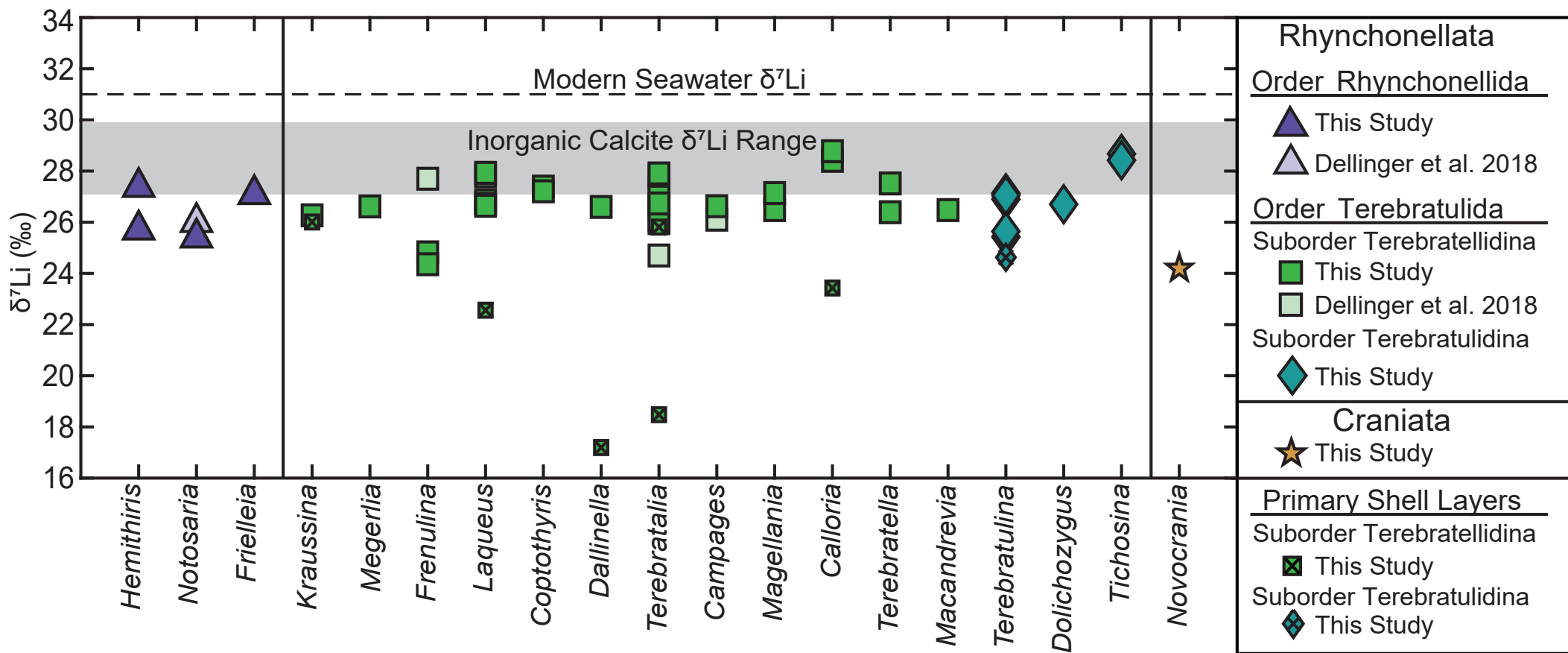


Fig. S1

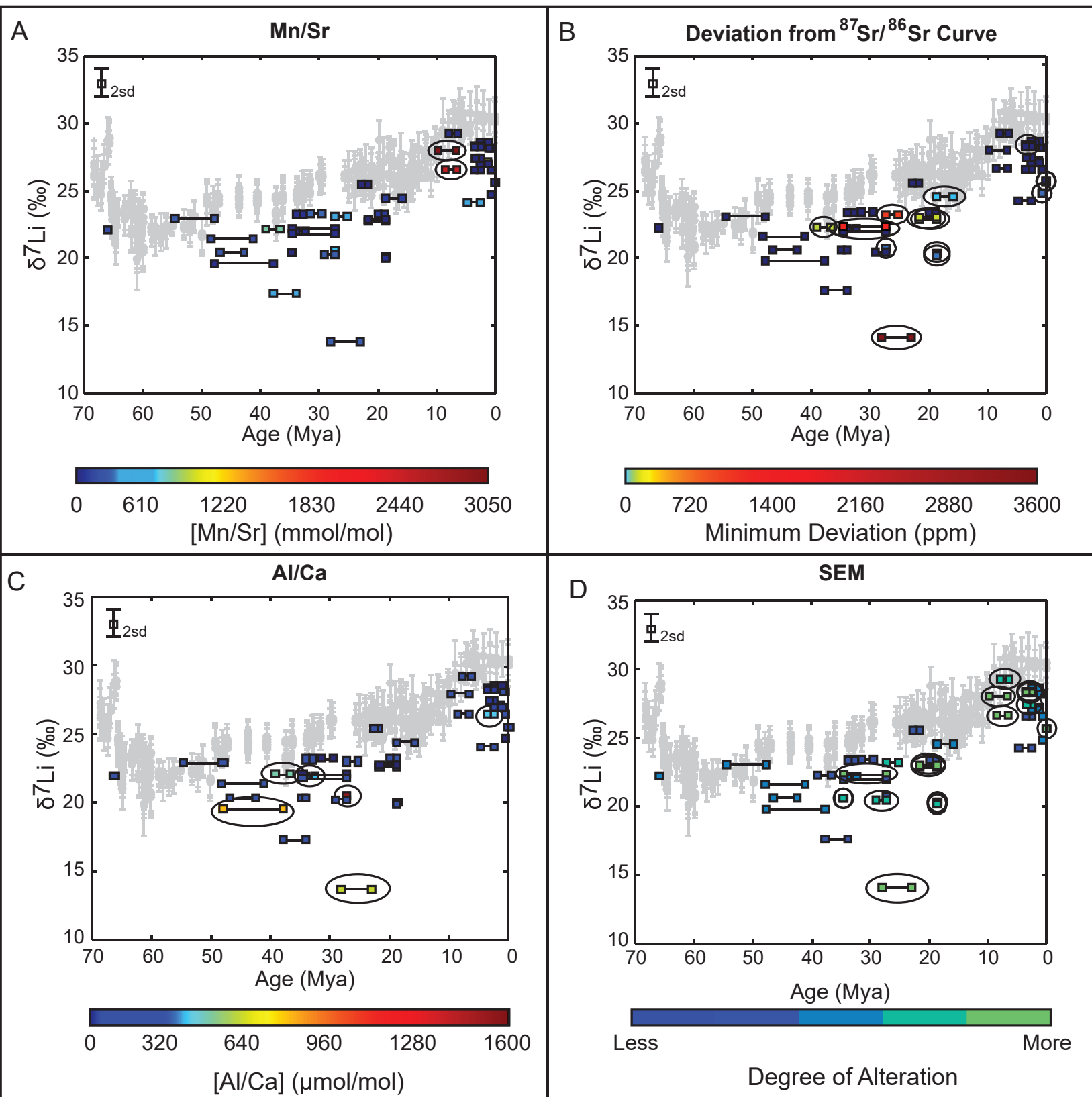


Fig. S2

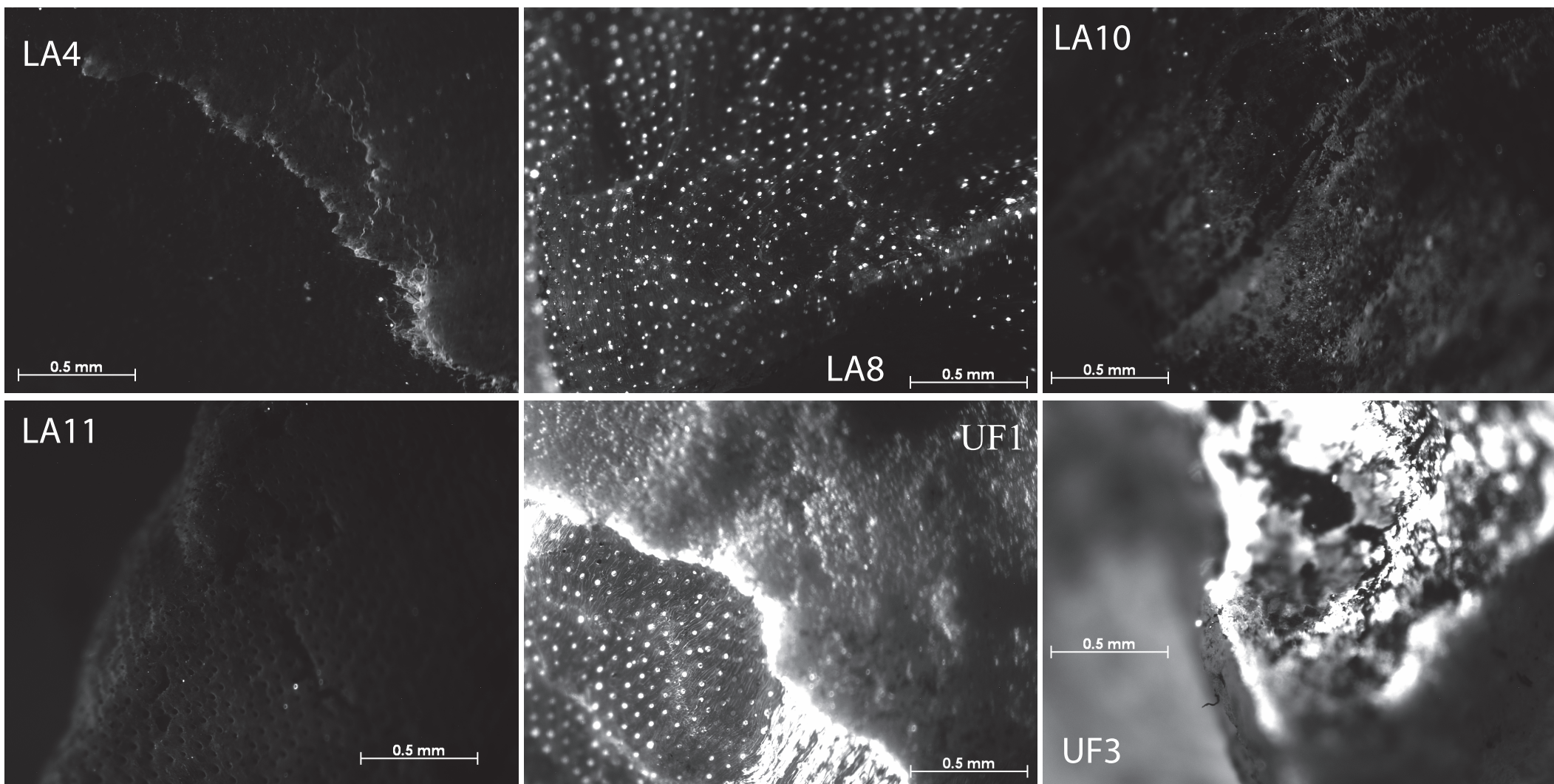
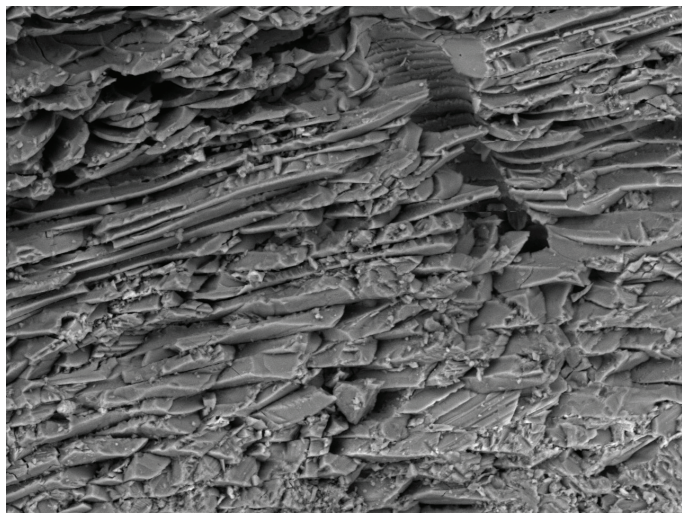
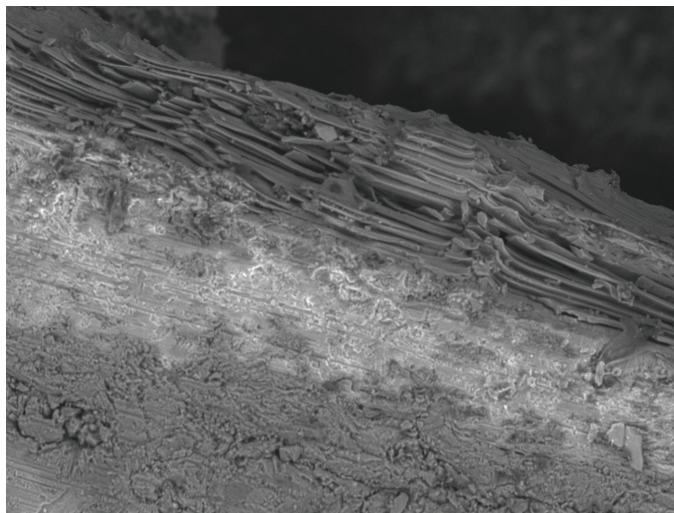


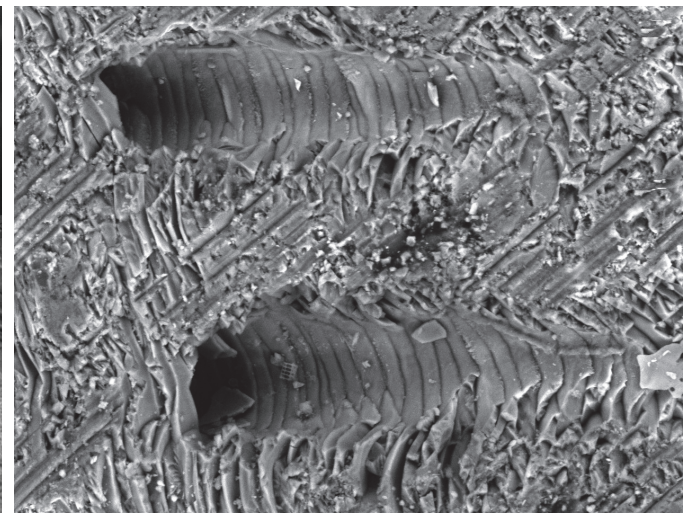
Fig. S3



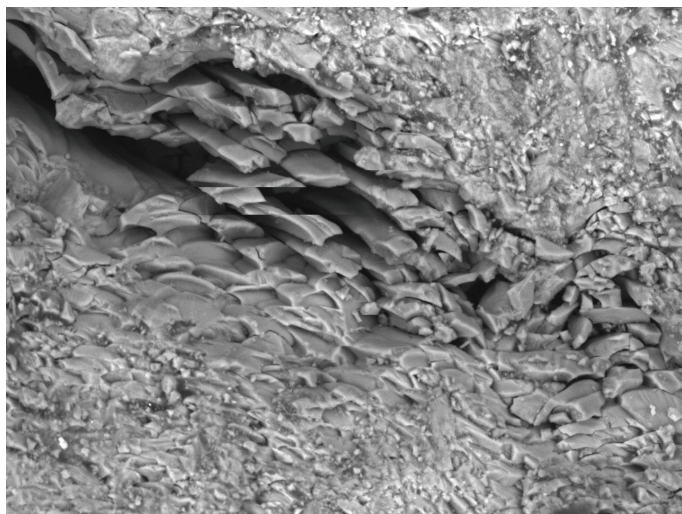
LA11 2018/04/23 13:18 x1.2k 50 um



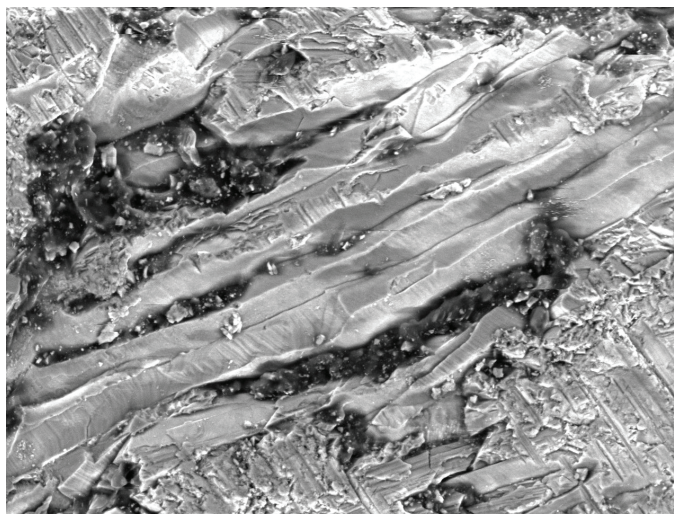
NZ7_A 2018/04/19 13:59 200 um



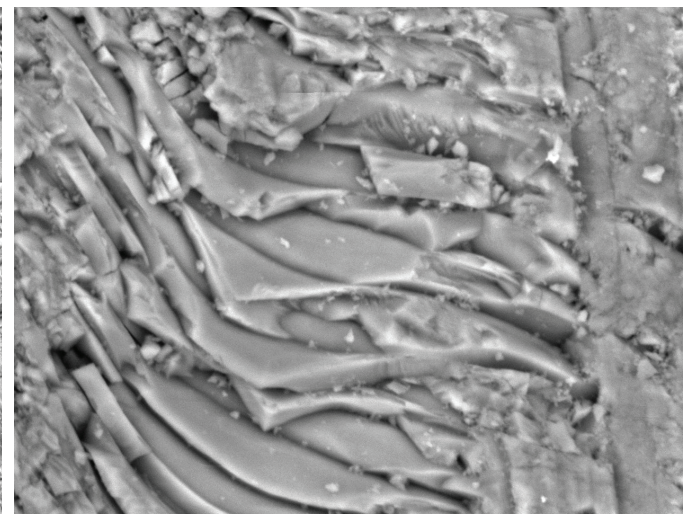
LA4 2018/04/23 11:55 x1.5k 50 um



UF1 2018/04/23 14:31 x1.5k 50 um



NZ4 2018/04/23 15:33 x1.2k 50 um



UF1 2018/04/23 14:28 x4.0k 20 um

Fig. S4

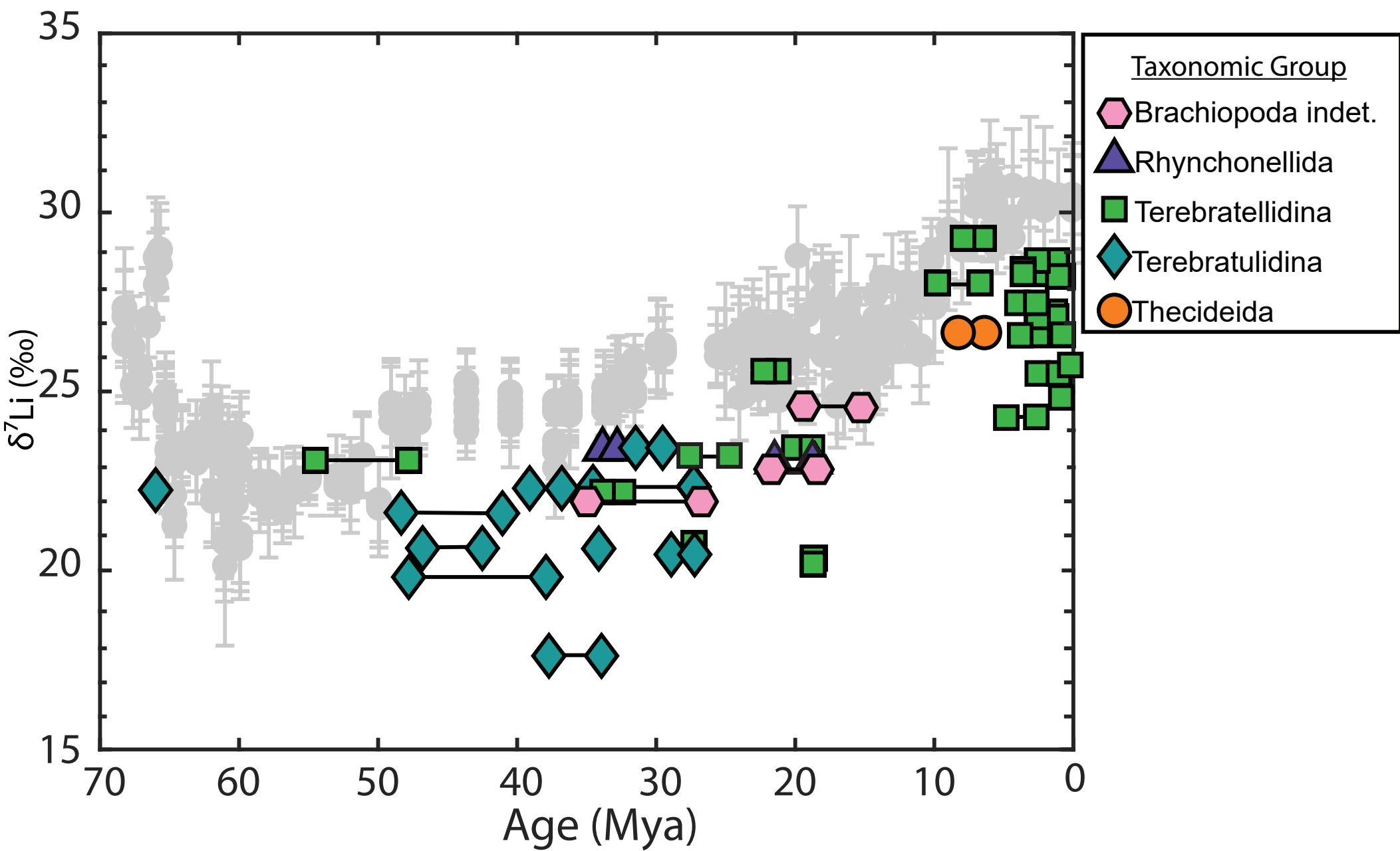
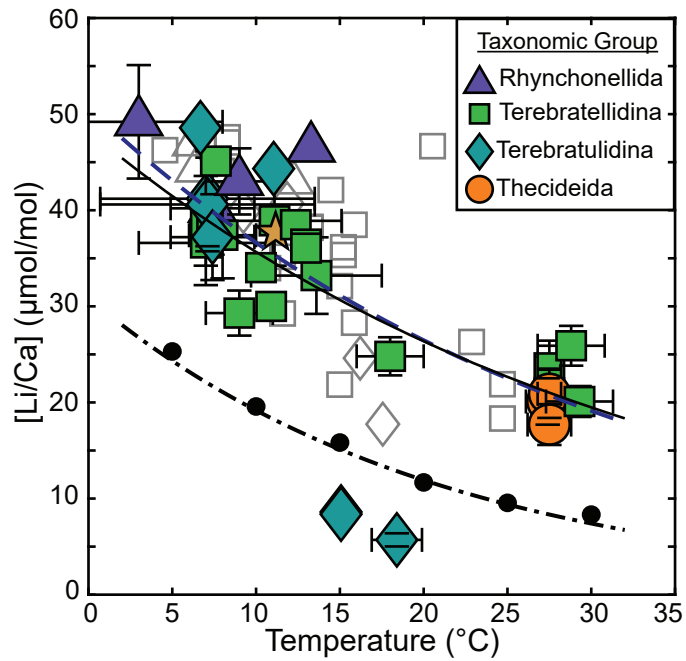


Fig. S5



<u>Synthetic Calcite (Marriott et al. 2004a)</u>	
- - - - Li/Ca = 31.9e ^{-0.05T} (R ² = 0.99)	
<u>Brachiopods</u>	
Delaney et al. 1989	
- - - - Li/Ca = 50.7e ^{-0.03T} (R ² = 0.95)	
This Study*; Literature Values	
— Li/Ca = 48.3e ^{-0.03T} (R ² = 0.75)	

Fig. S6

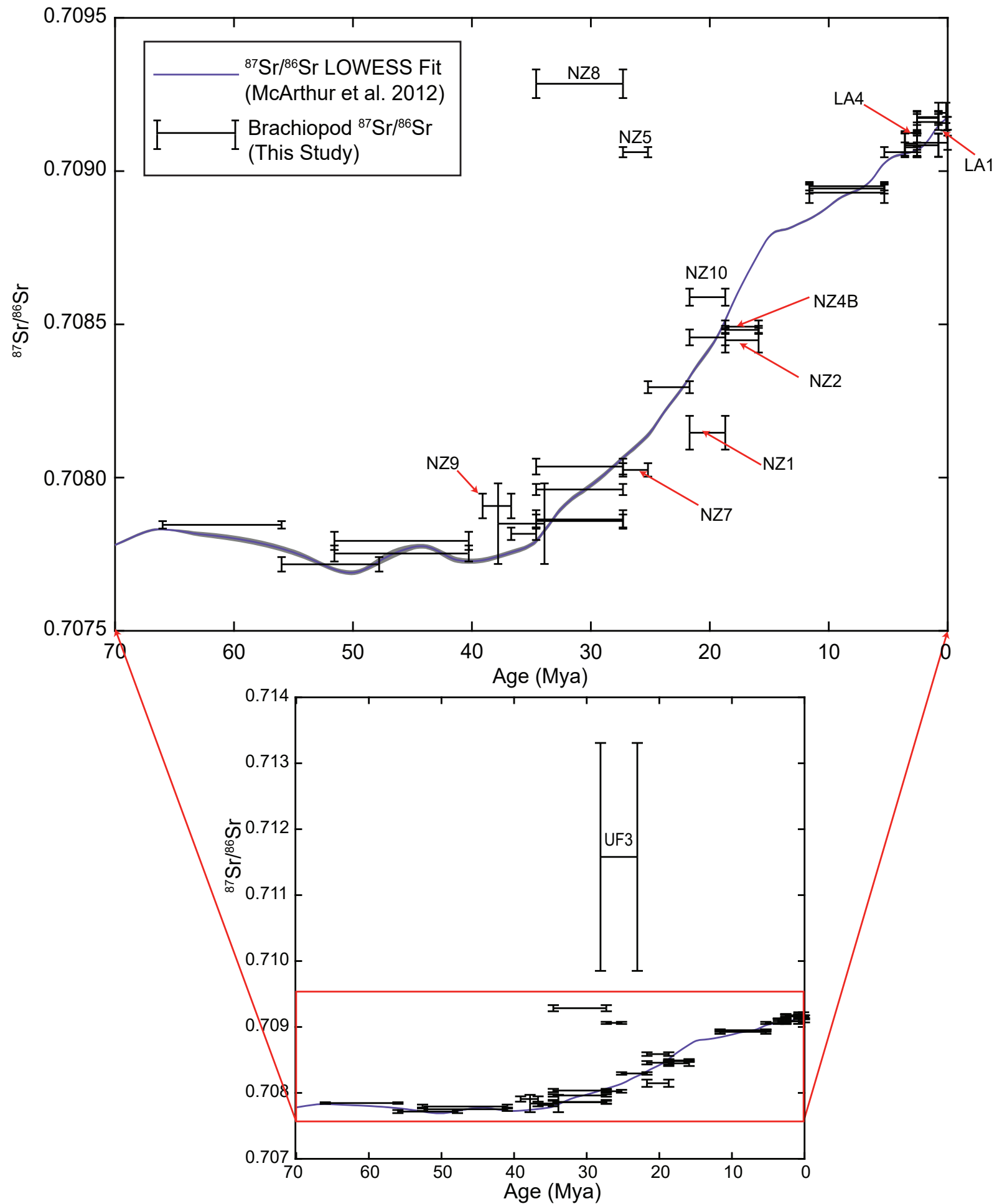


Fig. S7

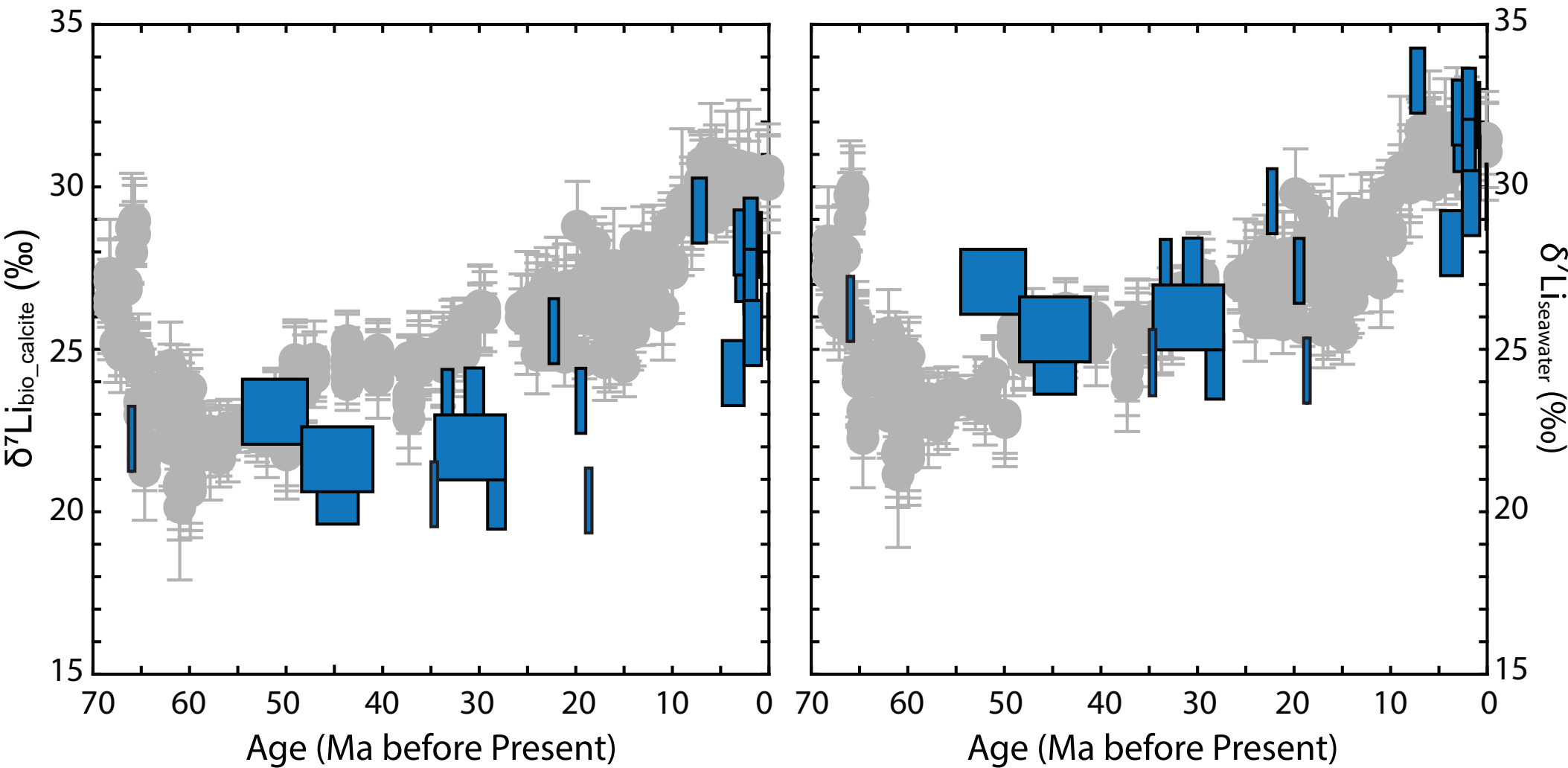


Fig. S8

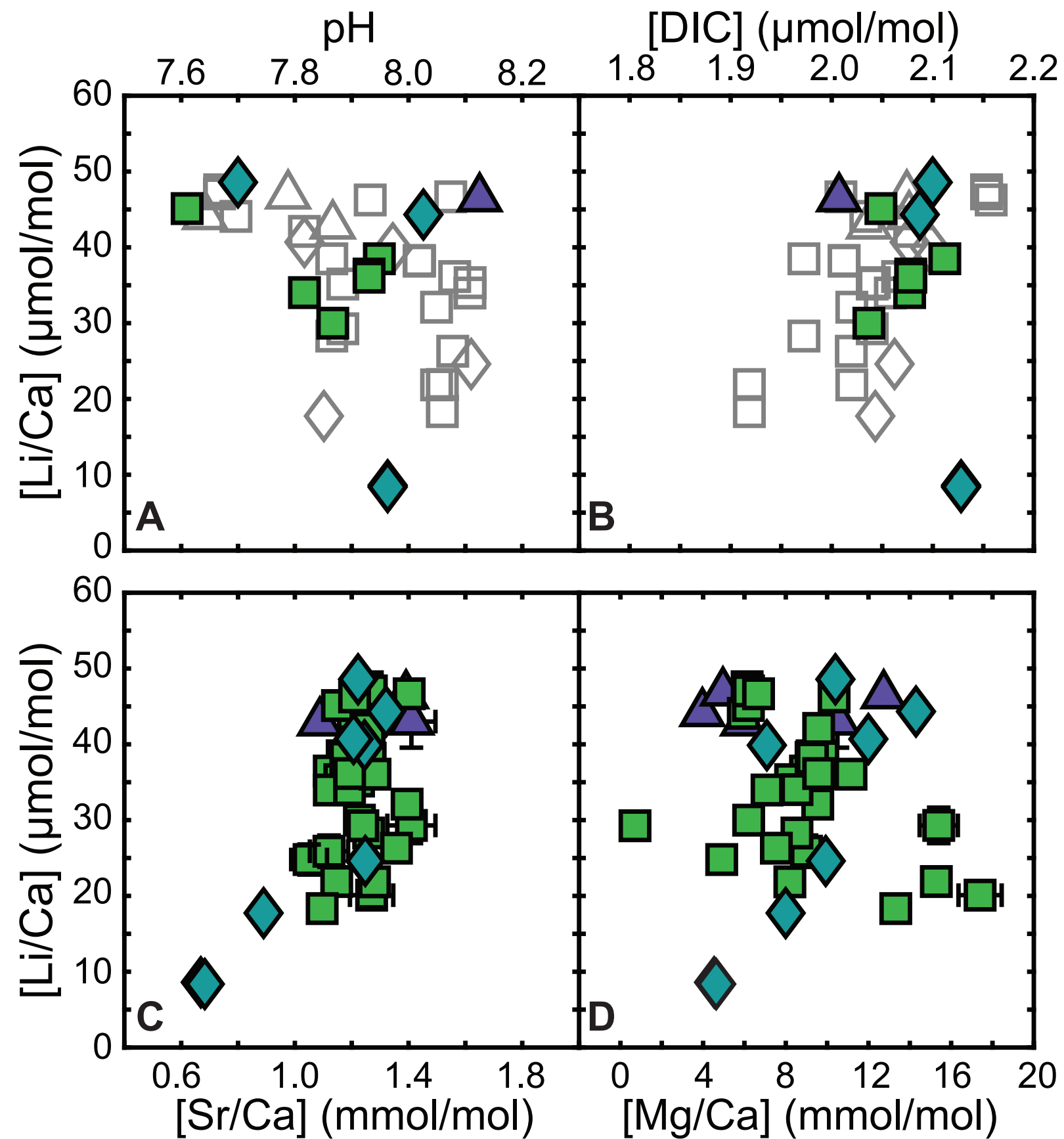


Fig. S9